Astron. Astrophys. 347, 112–118 (1999)

ASTRONOMY AND ASTROPHYSICS

Infrared line ratios revealing starburst conditions in galaxies

Sueli M. Viegas[1], **Marcella Contini**[1,2], **and Thierry Contini**[2,3]

[1] Instituto Astronômico e Geofísico, USP, Av. Miguel Stefano 4200, 04301-904 São Paulo, Brazil
[2] School of Physics & Astronomy, Tel Aviv University, 69978 Tel Aviv, Israel
[3] European Southern Observatory, Karl-Schwarzschild-Strasse 2, D-85748 Garching bei München, Germany

Received 29 October 1998 / Accepted 16 April 1999

Abstract. The physical conditions in typical starburst galaxies are investigated through critical infrared (IR) line ratios, as previously suggested by Lutz et al. (1998). The calculations by a composite model which consistently accounts for the coupled effect of shock and photoionization by hot stars definitely fit the observed line ratios of single objects and explain the observed relation between [O IV]/([Ne II]+0.44[Ne III]) and [Ne III]/[Ne II]. The shock velocity and the gas density are the critical parameters.

Most of the shocks are produced in low density-velocity ($n_0 \sim 100$ cm^{-3} and $V_\mathrm{s} \sim 50$–100 $\mathrm{km\,s}^{-1}$) clouds which represent the bulk of the ionized gas in starburst galaxies. However, though they are by many orders less numerous, high-velocity ($\sim$ 400–600 $\mathrm{km\,s}^{-1}$) shocks in dense ($\sim$ 500–800 cm^{-3}) clouds are necessary to reproduce the critical IR line ratios observed in the low-excitation Starburst Nucleus Galaxies (SBNGs: M 82, M83, NGC 253, NGC 3256, NGC 3690, and NGC 4945). These model predictions are in good agreement with the powerful starburst-driven superwinds and highly pressured ISM observed in SBNGs. On the contrary, the high-excitation HII galaxies (II Zw 40 and NGC 5253) do not show any clear signature of large scale outflows of gas. This difference between HII galaxies and SBNGs can be interpreted in terms of temporal evolution of their starbursts.

Key words: galaxies: starburst – galaxies: ISM – infrared: galaxies – line: formation – shock waves

1. Introduction

Detection of faint emission in the high excitation [O IV] 25.9 μm infrared (IR) line has been reported by Lutz et al. (1998) in a number of well-known starburst galaxies from observations with the Short Wavelength Spectrometer on board *ISO*.

IR line ratios such as [O IV] 25.9 μm / [Ne II] 12.8 μm and [O IV] 25.9 μm / [Ne III] 15.6 μm were used previously (Lutz et al., 1996; Genzel et al., 1998) to establish the dominant source (starburst or AGN) of ionizing radiations in ultraluminous infrared galaxies. Actually, rather than normalizing just to [Ne II] or [Ne III], Lutz et al. (1998) use [O IV]/([Ne II] + 0.44[Ne III]) as a critical line ratio to reveal different excitation conditions in starburst galaxies. Results from pure photoionization models or from pure shock models are used by these authors in order to explain the observed line ratios. However, these models were not successful in reproducing the IR line ratios of several starburst galaxies. In fact, models with a power-law radiation producing enough [O IV] line give too high values for the [Ne III]/[Ne II] line ratio. Those with two-temperature (39000 K + 80000 K) black body radiation fail in explaining the low-excitation starbursts. Finally, pure shock models could provide [O IV] line intensities similar to observations but not enough [Ne II] and [Ne III] which should come from the HII region.

These results indicate that a composite model, which accounts for the coupled effects of shocks and photoionization, must be used. Indeed, in a disturbed region such as that containing starbursts, it is expected that shocked gas is embedded in stellar radiation. This kind of composite model has successfully explained the AGN spectral features (Viegas & Contini 1997 and references therein) as well as those of single galaxies where the AGN and starburst activities are of comparable importance (e.g. the Circinus galaxy, Contini et al. 1998). These models were provided by the SUMA code (see Viegas & Contini 1994 and references therein).

In the present study we suggest that shocks result from supernova explosions in the nuclear starburst region of the galaxy, which provide enough kinetic energy to create high velocity superwinds. These in turn will accelerate gas clouds on large scales. The physical conditions in the ionized interstellar clouds are determined by shocks coupled to photoionization by massive hot stars (O and Wolf-Rayet).

This paper, rather than being an answer to Lutz et al. (1998), is aimed at carrying on their investigation. The distinction between AGN and starburst activity in galaxies being already established (Lutz et al., 1996; Genzel et al., 1998), our aim is to find out which models (provided by the SUMA code), better fit the observed trend between IR line ratios in starburst galaxies. We will not discuss in detail the single galaxy structures, but will use the fit of calculated to observed line ratios to define the critical parameters (and their ranges of values) which prevail in the emitting gas. In other words, we will treat the emission-line re-

Send offprint requests to: T. Contini (tcontini@eso.org)

Table 1. Parameters for single-cloud models

Galaxy	V_s ($km\,s^{-1}$)	n_0 (cm^{-3})	U	D (pc)
II Zw 40	50	100	0.02	0.10
NGC 5253	100	100	0.01	0.01
NGC 3690 B/C	300	100	0.01	0.03
NGC 3256	400	500	0.01	1.70
M 82	400	500	0.01	2.70
M 83	500	500	0.01	0.70
NGC 253	600	800	0.01	0.23
NGC 4945	600	800	0.01	0.20

gions of the observed galaxies as schematic systems of gaseous clouds moving radially outward from star-forming regions ionized by hot stars and shocks, avoiding a deep investigation on the internal structure of single objects.

2. The results by a composite model

As commented above, Lutz et al. (1998) concluded that shocks are the most plausible ionizing mechanism for explaining the [O IV] line, while the [Ne II] and [Ne III] come from the photoionized region. However, shock results should be obtained by consistent models concomitantly with photoionization from hot stars. The SUMA code consistently accounts for both the shock effect accompanying cloud expansion and photoionization by hot stars, in a plane-parallel symmetry. The geometrical thickness of the clouds range from 0.01 to 2.70 pc (see Table 1), which is small compared with the radius of the starburst regions in galaxies. In our model, we assume that the gas clouds move radially outward from the starburst region, i.e. the hot star population is facing the inner edges of the clouds while a shock develops on the opposite side.

For all models an average $stellar\,temperature$, T_*= 5×10^4 K, for the hot star population, and a preshock magnetic field, B_0 = 10^{-4} gauss, are adopted, as well as cosmic abundances. Lower abundances should lead to a lower cooling rate of the gas downstream which could be reajusted by adopting higher preshock densities. The other input parameters for SUMA: the shock velocity, V_s, the preshock density, n_0, the ionization parameter[1], U, and the geometrical thickness of the clouds, D, are chosen to vary within the ranges consistent with observations.

2.1. Single-cloud models

First we perform calculations by single-cloud models, which are compared with the observations of each galaxy in Fig. 1. The input parameters in the models are given in Table 1. Filled squares represent the data from the Lutz et al. (1998) sample and open squares the results of model calculations. Upper limits are not included. As shown in Lutz et al. (1998, Fig. 2) they

[1] The ionization parameter is the ratio of the photon density of the ionizing radiations reaching the nebula to the gas density in the inner part of the nebula.

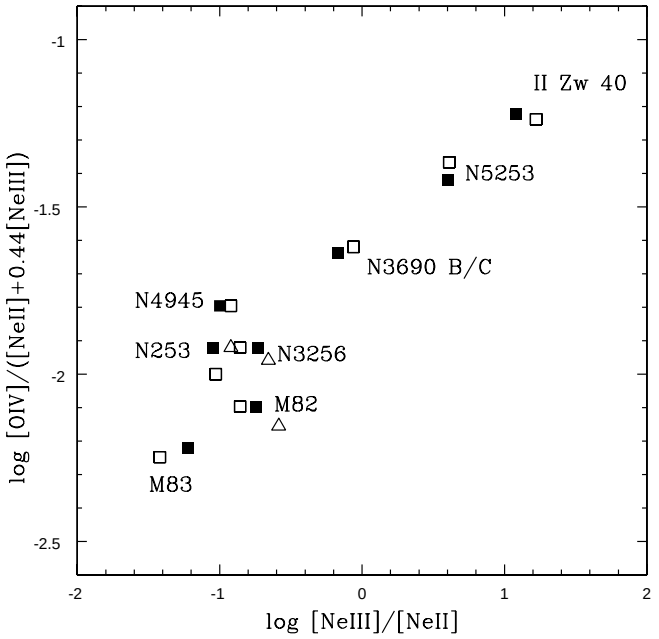

Fig. 1. [O IV] 25.9 μm / ([Ne II] 12.8 μm + 0.44 [Ne III] 15.5 μm) versus the [Ne III] 15.5 μm / [Ne II] 12.8 μm line ratio. The observational data from Lutz et al. (1998) are indicated by filled squares. Open symbols correspond to results for single-cloud (squares, input parameters listed in Table 1) and multiple-cloud (triangles, input parameters listed in Table 2) models.

are located in the left region of Fig. 1. The fit is very good for almost all galaxies. A perfect fit for individual data is senseless because many different conditions coexist in single objects. Notice indeed that NGC 4945 is a composite object with starburst/Seyfert 2 nuclear activity. This could explain its higher intensity of [O IV] 25.9 μm relative to model predictions for starburst only. A possible hidden AGN has also been reported in the merger galaxy NGC 3256 (Kotilainen et al., 1996).

The parameters listed in Table 1 indicate that the shock velocity and the preshock density are the critical parameters to reproduce the observed trend of the IR line ratios in Fig. 1. The velocity growth is generally followed by an increase of the preshock density. An ionization parameter of 0.01 was adopted for nearly all the models except for II Zw 40 for which $U = 0.02$. For this galaxy the effect of radiation dominates the shock effect (see Sect. 4). The geometrical thickness of the clouds, D, ranges between 0.01 pc for NGC 5253 and < 3 pc for M 82.

Lutz et al. (1998) already suggested that shocks are the most plausible source of [O IV] emission observed in starburst galaxies. Our results show that shocks are also necessary to reproduce the low observed values of [Ne III]/[Ne II] (see Sect. 3 for details). Moreover, Fig. 1 shows that the objects with [Ne III]/[Ne II] < 1 are well fitted by models characterized by high velocity and density clouds. However, previous investigations on the physical conditions in the ISM of NGC 253 (Carral et al., 1994), NGC 3256 (Carral et al., 1994; Rigopoulou et al., 1996), and M 82 (Houck et al., 1984; Lord et al., 1996) found relatively low

Table 2. Calculated line fluxes (in $\mathrm{erg\,cm^{-2}\,s^{-1}}$) with multi-cloud models

Line	M 82					NGC 3256				NGC 253			
(μm)	A1	A2	A3	A4	Av	B1	B2	B3	Av	C1	C2	C3	Av
[C II] 158	0.05	0.026	0.007	0.420	2.56	0.03	0.012	0.007	1.6	0.03	0.07	6×10^{-4}	7.06
	0.01	16.5	27.0	56.5	–	0.04	75	24.5	–	0.02	99.1	0.85	–
[O III] 88	9.6	0.002	0.008	0.001	0.92	6.2	0.002	0.008	0.8	2.10	3×10^{-5}	0.0076	0.78
	6.30	4.2	89.0	0.39	–	13.9	23.8	62.4	–	11.3	0.3	88.5	–
[O I] 63	0.004	0.067	0.007	0.348	2.96	0.002	0.025	0.007	2.9	0.78	0.075	5×10^{-4}	7.59
	0.0008	37.0	23.0	40.0	–	0.002	86.5	13.5	–	0.5	98.8	0.66	–
[O III] 52	89.6	0.004	0.008	0.003	1.46	56.6	0.004	0.008	2.0	20	6.7×10^{-5}	0.0078	1.73
	36.7	4.5	57.8	0.9	–	54.6	20.4	26.5	–	53.7	0.4	45.7	–
[Si II] 35	25.6	0.166	0.027	2.170	13.20	15.9	0.073	0.027	9.4	3.70	0.44	0.01	45.2
	1.2	20.8	20.5	57.6	–	3.2	77.4	19.4	–	0.4	97.4	2.2	–
[S III] 33	12.0	0.055	0.001	0.570	3.10	7.5	0.024	0.001	2.6	3.30	0.02	2×10^{-4}	2.17
	2.3	29.3	4.2	64	–	5.5	91.6	3.0	–	7.1	91.9	0.92	–
[S III] 18	96.0	0.031	6.6×10^{-4}	0.114	1.54	60.6	0.013	6.6×10^{-4}	2.5	30	0.005	1.2×10^{-5}	1.85
	1.9	32.9	4.2	25.8	–	46.2	52.2	0.02	–	75	24.5	0.64	–
[O IV] 25.9	7	1.2×10^{-4}	6.6×10^{-5}	2.3×10^{-4}	0.05	7	1.2×10^{-4}	6.6×10^{-5}	0.14	5.6	8.8×10^{-5}	6.3×10^{-5}	0.3
	82	4	13	1	–	89	8	3	–	94	3	2	–
[Ne III] 15.5	123	0.014	0.008	0.01	1.80	80	0.0075	0.008	2.77	46	8×10^{-4}	0.0063	2.8
	40	13	45	2	–	55	27	18	–	75	3	22	–
[Ne II] 12.8	960	0.025	0.004	0.15	7.06	606	0.01	0.004	12.6	490	0.0055	0.0016	23.3
	82	6	5	7	–	90	8	2	–	97	2	0.7	–
W (%)	0.005	13.8	83.3	2.895	–	0.01	60.4	39.59	–	0.007	49.493	50.5	–
V_S ($\mathrm{km\,s^{-1}}$)	400	200	100	200	–	400	200	100	–	600	100	100	–
n_0 ($\mathrm{cm^{-3}}$)	500	50	40	100	–	500	50	40	–	800	200	40	–
U	0.01	0.01	0.01	0.01	–	0.01	0.01	0.01	–	0.01	0.001	0.01	–
D (pc)	2.67	3.33	3.33	20	–	1.67	1.67	3.33	–	0.23	10	0.5	–

For each line, we report as a second entry the percentage contribution of each model in the weighted sum flux.

Table 3. Observed vs. calculated IR line fluxes[a]

Line	NGC 253		NGC 3256		M 82	
(μm)	Obs[b]	Cal	Obs[b]	Cal	Obs[b]	Cal
[O III]88	0.10±0.02	0.1	0.4±0.3	0.5	0.6±0.2	0.4
[O I]63	0.9±0.1	1.0	1.2±0.4	1.7	1.1±0.4	1.2
[O III]52	0.20±0.04	0.2	<1.3	1.2	0.7±0.2	0.5
[Si II]35	1.1±0.2	6.2	1.9±0.5	5.6	1.0±0.4	5.4
[S III]33	<1.3	0.3	1.2±0.3	1.6	1.1±0.3	1.2
[S III]18	...	0.2	0.9±0.2	1.5	0.7±0.3	0.6

[a] Fluxes are relative to [C II] 158 μm.
[b] Observed line fluxes from Carral et al. (1994) for NGC 253 and NGC 3256, Rigopoulou et al. (1996) for NGC 3256, and Lord et al. (1996) for M 82.

electronic densities on the basis of the [S III] 33 μm/18 μm and [O III] 88 μm/52 μm line ratios, and low velocities derived from the FWHM of the IR line profiles.

2.2. Multi-cloud models

Many different conditions coexist in the ISM of single galaxies. Therefore, we performed multi-cloud model calculations to reproduce all the observed IR line ratios available in the literature for the starburst galaxies NGC 253, NGC 3256, and M 82. In these models, we assume that both *low* and *high* density-velocity (d-v) clouds are present in single objects.

In Table 2, the calculated IR line fluxes are given for single-cloud models and for the weighted sums of the multi-cloud models. Notice that the line fluxes are calculated at the emitting nebula while the observations are given at Earth. The input parameters of single-cloud models are also listed.

Line fluxes are proportional to the square of the gas emitting density, and compression downstream increases with the shock velocity. Thus, the line fluxes computed from high d-v models (i.e. A1, B1, and C1) are higher than those calculated from low d-v models (A2, A3, A4, B2, B3, C2, and C3) by some orders of magnitude, except for lines [O I] and [C II]. The gas in high d-v models is ionized to very high temperatures (Fig. 3b), and so low-level lines like [O I] and [C II] are weak. Recall that the first ionization potential of C is lower than that of H (and Ne). Consequently, [C II] lines, as well as [O I] lines, are emitted by relatively cold gas and can be weak in models which show strong [Ne II] lines.

In order to fit the observations, a balance must be achieved between high and low d-v models in the multi-cloud spectra, and the final result is a weighted sum (A_v in Table 2) with the weights chosen adequately. For each model, the weight W represents the relative number of clouds (in%) characterized by that model. The weights of low d-v models must be by a factor of 10^4–10^5 higher than for high d-v models. In other words, the number of high d-v clouds must be very low compared with the number of low d-v clouds. In Table 2, for each emission line, the second entry corresponds to the percentage contribution of the single-cloud model to the line flux, taking into account the corresponding weight. The high d-v clouds contribute up to 90% to the [O IV] and [Ne II] emission lines, whereas the [Ne III] line is produced at a same level both by low and high d-v clouds for M 82 and NGC 3256. The others IR lines are mainly emitted by the low d-v clouds except the [O III] 52 line.

The results of multi-cloud model calculations are compared to the observed IR line ratios in Table 3 and plotted in Fig. 1 (open triangles). The fit is good for all line ratios (especially for the density critical ones, see Sect. 2.1), except for the [Si II] line

which is overpredicted by a factor of about 5. This might indicate that silicium is depleted and locked in dust grains. Adopting a relative abundance Si/H lower by a factor of ~ 5 than cosmic will not affect the predictions for the other line ratios listed in Table 3. Most of the IR lines reported in Table 2 (e.g. [O I], [C II], etc) are mainly produced by the low d-v clouds. Thus, in the weighted sum, the IR lines ratios [S III] 33 μm/18 μm and [O III] 88 μm/52 μm are determined by low d-v models, while the [O IV]/([Ne II]+0.44[Ne III]) and [Ne III]/[Ne II] line ratios are mainly determined by the high d-v cloud component.

Once fitted the line ratios, it is now possible to examine the FWHM of the line profiles, because the weights adopted in Table 2 for high d-v models are very low and could lead to hardly observable broad components in the line profiles. The calculated line profiles for M 82 and NGC 253 are shown in Fig 2. The effect of galaxy rotation is included in the calculation. Rotation velocities are about 76 $\mathrm{km\,s^{-1}}$ and 189 $\mathrm{km\,s^{-1}}$ for M 82 and NGC 253 respectively. Two significant lines are chosen for each galaxy: [O IV] and [Ne III] for M 82, and [O IV] and [O III] 88 for NGC 253. The [O III] 88 line is chosen because it represents the case of a low contribution of the high d-v model (C1) relatively to a strong contribution of the low d-v model (C3). Single-cloud model profiles are also plotted in the figures using their percentage contribution reported in Table 2. The broad component from the high d-v clouds dominates the weighted averaged profile of [O IV], while in the [O III] 88 and [Ne III] profiles the broad component is faint and hardly observable, due to the low contribution from high d-v clouds. For M 82, the predicted FWHM of the [O IV] profile is ~ 300 $\mathrm{km\,s^{-1}}$, in good agreement with the observed value (FWHM $\sim$ 360 $\mathrm{km\,s^{-1}}$) reported by Lutz et al. (1998).

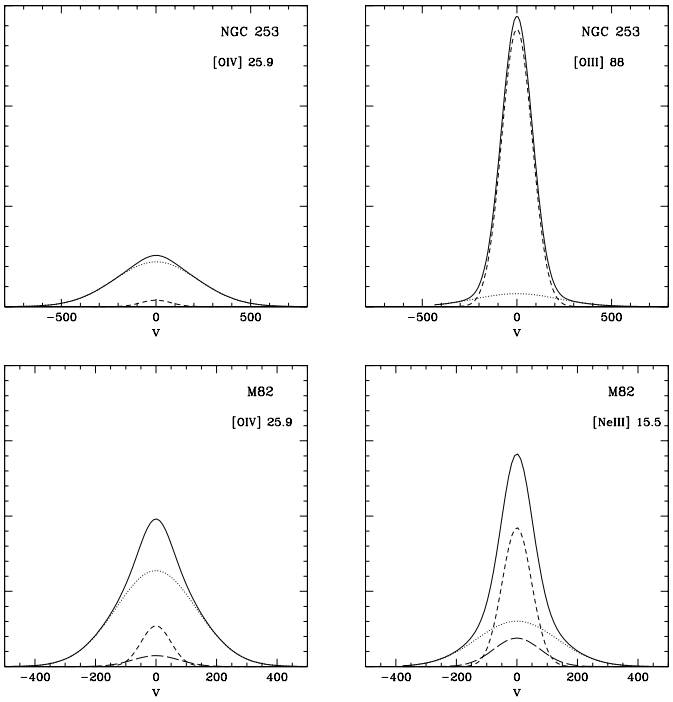

Fig. 2. Predicted line profiles for NGC 253 (*top*) and M 82 (*bottom*) using multi-cloud models. The final profile (solid line) is the weighted sum of different cloud components: high density-velocity clouds (dotted line) and low density-velocity clouds (long-dashed line: V_s = 200 $\mathrm{km\,s^{-1}}$; short-dashed line: V_s = 100 $\mathrm{km\,s^{-1}}$)

3. The physical conditions across emitting clouds

To better understand the role of the input parameters in determining the physical conditions of the emitting gas, the distribution of some important physical quantities across the cloud is given in Figs. 3a and 3b respectively for two significant models listed in Table 1: NGC 5253, which represents the low density-velocity cloud component, and the high density-velocity component of NGC 253. Each figure shows three panels where the shock front is on the left and the photoionized edge is on the right. The top panel displays the electron temperature, T_e, and density, n_e. The fractional abundances of the ions $\mathrm{O^{+3}/O}$, $\mathrm{Ne^{+2}/Ne}$, and $\mathrm{Ne^{+1}/Ne}$ are shown in the central panel. The ionization rates for $\mathrm{Ne^{+2}}$ due to the primary radiation (P), to the diffuse radiation (D), and to electronic collisions (C) are given in the bottom panel.

The [O IV] line is always emitted from the shock dominated region where the temperatures are high, with no contribution from the photoionized zone. In particular, Fig. 3a shows that the critical temperatures are about 10^5 K. For NGC 5253 the shock effect becomes negligible at a distance of about 10^{15} cm from the shock front, and most of the physical conditions in the cloud are then dominated by the effect of stellar radiation which leads to [Ne III]/[Ne II] > 1. On the other hand, due to strong compression in the NGC 253 gas clouds (Fig. 3b), the temperature rapidly drops to $T_\mathrm{e} < 10^4$ K. This can be explained by the high density ($\sim 10^5$ $\mathrm{cm^{-3}}$) of the gas in the innermost region of the cloud which strengthens the cooling rate. The role of the primary radiation is to keep the gas at a temperature slightly below 10^4 K corresponding to a relatively high $\mathrm{Ne^{+1}/Ne}$ compared to $\mathrm{Ne^{+0}/Ne}$ and $\mathrm{Ne^{+2}/Ne}$. Therefore, for this galaxy, [Ne III]/[Ne II] is < 1. Owing to the high optical thickness of the gas, the stellar radiation flux reaching the inner edge of the cloud rapidly decreases, the size of the $\mathrm{Ne^{+2}}$ photoionized zone is reduced, and the diffuse radiation effect prevails accross the cloud.

For NGC 253, temperatures as high as 7×10^6 K deduced from the ROSAT PSPC data (Heckman 1996 and references therein) are in agreement with 5.4×10^6 K obtained by the model in the postshock region (Fig. 3b). Precursor soft X-rays radiation from the hot gas could affect the ionization conditions in the upstream gas clouds. However, due to the adiabatic jump and compression, the densities n upstream are lower than in the downstream gas by at least a factor of 4. Considering that line intensities depend on n^2, the contribution of the line emission from upstream gas to the final spectrum will be small.

4. Comparison with the observed starburst properties

One might interpret the observed trend in Fig. 1 as a continuous sequence between two extreme cases: starburst regions where

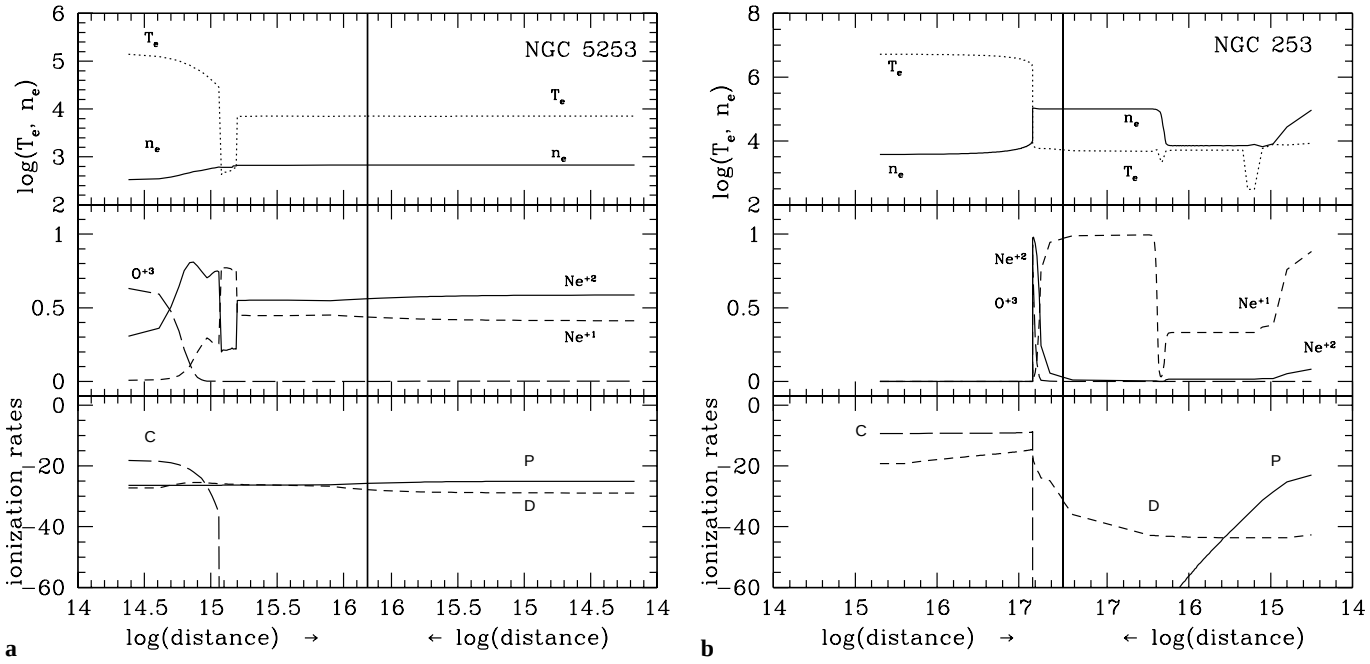

Fig. 3a and b. The physical conditions across low-density (**a**, NGC 5253) and high-density (**b**, NGC 253) clouds are shown in three panels, each one with a vertical line indicating the center of the emitting clouds. The electron temperature (dotted line) and electron density (solid line) appear in the *top panel*. The fractional abundances of O^{+3} (long-dashed line), Ne^{+2} (solid line), and Ne^{+1} (short-dashed line) are displayed in the *central panel*. The ionization rates for Ne^{+2} (in logarithmic units) due to electron collisions C (long-dashed line), to the stellar radiation P (solid line) and to the diffuse radiation D (short-dashed line) are shown in the *bottom panel*. The shock front is on the left side and the edge of the cloud photoionized by the stellar radiation is on the right of each panel. The horizontal axis scale is logarithmic and symmetric in order to show an equal view of both sides of the emitting cloud

shocks in high-velocity clouds are *necessary* to reproduce the observed critical IR line ratios (bottom left part of the diagram) and the "radiation-dominated" ones (upper right part of the diagram), where the shock contribution is relatively less important, because formed only in low-velocity clouds. Let us now check wether the critical parameters derived from the models along this sequence are in agreement with the observed properties of the starburst galaxies.

Galaxies in the first group (the last six galaxies in Table 4) are massive and chemically evolved spiral galaxies which exhibit a single energetic and compact starburst in their nucleus, and are commonly named Starburst Nucleus Galaxies (SBNGs; Balzano 1983; Coziol et al. 1994). Evidence for powerful large-scale starburst-driven superwinds in the nuclear region of SBNGs (like M 82, NGC 253, NGC 4945 and NGC 3690 in the present sample) has been reported by Heckman et al. (1990). Moreover, the strong X-ray emission ($L_{\rm X} \sim 10^{40} - 10^{42}$, see Table 4) in SBNGs provides strong evidence for the formation of hot superbubbles due to the combined action of stellar winds from massive stars and supernova explosions in the central starburst cluster. Expanding velocities as high as $\sim$ 500–600 $\rm km\,s^{-1}$ have been estimated for the ionized gas in M 82 (Shopbell & Bland-Hawthorn, 1998), NGC 4945 (Moorwood et al., 1996), and NGC 253 (Heckman, 1996).

In the central region of SBNGs, part of the ISM is overpressured relative to the ISM in the Milky Way

Table 4. Galaxian properties

Galaxy	Morph.[a]	$M^{\rm a}_{\rm abs}$	$d^{\rm b}$ (Mpc)	$\log L^{\rm b}_{\rm X}$ ($\rm erg\,s^{-1}$)
II Zw 40	BCDG	−14.5	9.2	...
NGC 5253	Irr	−16.2	4.1	38.6
NGC 3690 B/C	Merger	−21.1	42.4	41.0
NGC 3256	Merger	−22.2	33.2	41.7
M 82	Sd	−19.0	4.3	39.7
M 83	SABc	−21.2	5.1	40.2
NGC 253	SABc	−20.9	3.3	39.9
NGC 4945	SBcd	−20.1	5.1	39.9

[a] From the LEDA database
[b] The distance (d) is derived from the Galactic Standard of Rest (GSR) velocity, using a Hubble constant $H_0 = 75\,\rm km\,s^{-1}$ $\rm Mpc^{-1}$, except for the distance of NGC 5253 taken from Saha et al. (1995). The X-ray luminosity is derived from the flux reported in the *ROSAT* catalog (Brinkmann et al. 1994) or in the *EINSTEIN* catalog (Fabbiano et al. 1992).

(Heckman et al., 1990; Carral et al., 1994), due to compression by superwinds. The nuclear starbursts usually contain many compact radio sources associated with bright and small supernova remnants (Muxlow et al. 1994; Huang et al. 1994 for M 82; Ulvestad & Antonucci 1997 for NGC 253; Zhao et al. 1997 for NGC 3690). Such a population of dense and compact objects

is generally attributed to the high pressure in the central region of SBNGs which allows the formation of dense ionized clouds (see e.g. Carilli 1996).

The galaxies in the second group (the first two galaxies in Table 4) are mostly metal-poor dwarf irregular galaxies with multiple star-forming regions distributed randomly, and are known as HII galaxies (French, 1980). The archetypes of this class of galaxies are II Zw 40 and NGC 5253. Their starbursts are very young (≤ 4 Myr), as proved by the numerous Wolf-Rayet stars still present in II Zw 40 (Kunth & Sargent, 1981; Vacca & Conti, 1992) and NGC 5253 (Schaerer et al., 1997; Schaerer et al., 1999), and only contain a few supernova remnants (Vanzi et al. 1996 for II Zw 40; Beck et al. 1996 for NGC 5253). Moreover, there is no evidence for powerful starburst-driven superwinds in these galaxies (Martin 1998 for II Zw 40; Marlowe et al. 1995 for NGC 5253) which are faint or even undetected in X-rays (see Table 4).

Thus, the distinction between HII galaxies and SBNGs can be understood in terms of temporal evolution of the starbursts. In the former galaxies (II Zw 40 and NGC 5253), the star-forming event is still young enough to contain a high proportion of massive O and Wolf-Rayet stars. These populations of hot ($T_{\rm eff} \sim 60000$ K) stars produce large amounts of ionizing radiation, but did not have the time to evolve off the main sequence to produce supernova explosions. In SBNGs, like M 82 or NGC 253, the starburst is much older (≥ 20 Myr, e.g. Engelbracht et al. 1998), and the most massive stars had the time to evolve through supernovae. As shown by the models of Leitherer & Heckman (1995), the ratio between the mechanical energy and the ionizing Lyman continuum, both injected in the ISM by the massive star population, rapidly increases by a factor of ~ 100 between ~ 5 and 20 Myr. This explain the difference between the "radiation-dominated" HII galaxies and the "shock-dominated" SBNGs. The presence of high density-velocity clouds in SBNGs, which host a relatively "old" starburst, require large quantities of mechanical energy to power large-scale superwinds. These energetic events disrupt molecular clouds through shock waves and drive them out of the nucleus at high velocities.

5. Conclusions

The observed relation between [O IV]/([Ne II]+ 0.44[Ne III]) and [Ne III]/[Ne II], and single object IR line ratios are well reproduced by models accounting consistently for both shock and photoionization effects occurring in starburst regions. The critical parameters which reproduce the observed trend of the IR line ratios are the preshock density and the shock velocity which are consistently correlated. Most of the shocks are produced in low density-velocity ($n_0 \sim 100\,{\rm cm}^{-3}$ and $V_{\rm s} \sim 50$–$100\ {\rm km\,s}^{-1}$) clouds which represent the bulk of the ionized gas in starburst galaxies. However, even if they are by many orders less numerous, high-velocity (~ 400–$600\ {\rm km\,s}^{-1}$) shocks in dense (~ 500–$800\ {\rm cm}^{-3}$) clouds are necessary to reproduce the critical IR line ratios observed in the low-excitation SBNGs.

These model predictions are in good agreement with the observed ISM properties in starburst galaxies. SBNGs are the only ones to exhibit powerful starburst-driven superwinds and highly pressured ISM. On the contrary, the high-excitation HII galaxies do not show any clear signature of large scale outflows of gas. This difference between HII galaxies and SBNGs can be interpreted in terms of temporal evolution of their starbursts. In the former, the starburst is too young to release large amounts of mechanical energy through supernova explosions whereas in the latter, characterized by older starbursts, the kinetic energy compete with the ionizing radiation in the heating of the ISM.

Acknowledgements. M.C. is grateful to the Instituto Astronômico e Geofísico, USP for warm hospitality. We thank Emmanuel Davoust for a careful reading of the manuscript and the anonymous referee for helpful comments and suggestions. This research has made use of the Lyon-Meudon Extragalactic Database (LEDA) supplied by the LEDA team at the CRAL - Observatoire de Lyon (France). This work was partially supported by FAPESP and PRONEX/Finep, Brazil.

References

Balzano V.A., 1983, ApJ 268, 602
Beck S.C., Turner J.L., Ho P.T.P., Lacy J.H., Kelly D.M., 1996, ApJ 457, 610
Brinckmann W., Siebert J., Boller Th., 1994, A&A 281, 355
Carilli C.L., 1996, A&A 305, 402
Carral P., Hollenbach D.J., Lord S.D., et al., 1994, ApJ 423, 223
Contini M., Prieto M.A., Viegas S.M., 1998, ApJ 505, 621
Coziol R., Demers S., Peña M., Barnéoud R., 1994, AJ 108, 405
Engelbracht C.W., Rieke M.J., Rieke G.H., Kelly D.M., Achtermann J.M., 1998, ApJ 505, 639
Fabbiano G., Kim D.-W., Trinchieri G., 1992, ApJS 80, 531
French H.B., 1980, ApJ 240, 41
Genzel R., Lutz D., Sturm E., et al., 1998, ApJ 498, 579
Heckman T.M., 1996, In: Kunth D., Guiderdoni B., Heydary-Malayeri M., Trinh Xuan Thuan (eds.) The Interplay between Massive Star Formation, the ISM and Galaxy Evolution. Editions Frontiers, p. 159
Heckman T.M., Armus L., Miley G.K., 1990, ApJS 74, 833
Houck J.R., Shure M.A., Gull G.E., Herter T., 1984, ApJ 287, L11
Huang Z.P., Thuan T.X., Chevalier R.A., Condon J.J., Yin Q.F., 1994, ApJ 424, 114
Kotilainen J.K., Moorwood A.F.M., Ward M.J., Forbes D.A., 1996, In: Kunth D., Guiderdoni B., Heydary-Malayeri M., Trinh Xuan Thuan (eds.) The Interplay between Massive Star Formation, the ISM and Galaxy Evolution. Editions Frontiers, p. 541
Kunth D., Sargent W.L.W., 1981, A&A 101, L5
Leitherer C., Heckman T.H., 1995, ApJS 96, 9
Lord S.D., Hollenbach D.J., Haas M.R., et al., 1996, ApJ 465, 703
Lutz D., Genzel R., Sternberg A., et al., 1996, A&A 315, L37
Lutz D., Kunze D., Spoon H.W.W., Thornley M.D., 1998, A&A 333, L75
Marlowe A.T., Heckman T.M., Wyse R.F.G., 1995, ApJ 438, 563
Martin C.L., 1998, ApJ 506, 222
Moorwood A.F.M., van der Werf P.P., Kotilainen J.K., Marconi A., Oliva E., 1996, A&A 308, L1
Muxlow T.W.B., Pedlar A., Wilkinson P.N., et al., 1994, MNRAS 266, 455
Rigopoulou D., et al., 1996, A&A 315, L125

Saha A., Sandage A., Labhardt L., et al., 1995, ApJ 438, 8
Schaerer D., Contini T., Kunth D., Meynet G., 1997, ApJ 481, L75
Schaerer D., Contini T., Kunth D., 1999, A&A 341, 399
Shopbell P.L., Bland-Hawthorn J., 1998, ApJ 493, 129
Ulvestad J.S., Antonucci R.R.J., 1997, ApJ 488, 621
Vacca W.D., Conti P., 1992, ApJ 401, 543
Vanzi L., Rieke G.H., Martin C.L., Shields J.C., 1996, ApJ 466, 150
Viegas S.M., Contini M., 1994, ApJ 428, 113
Viegas S.M., Contini M., 1997, In: Emission Lines in Active Galaxies: New Methods and Techniques. IAU Colloquium N.159
Zhao J-H., Anantharamaiah K.R., Goss W.M., Viallefond F., 1997, ApJ 482, 186